Speich, L., Kohn, S. C., Wirth, R., Bulanova, G. P., & Smith, C. B. (2017). The relationship between platelet size and the B infrared peak of natural diamonds revisited. *Lithos*, *278-281*, 419–426. https://doi.org/10.1016/j.lithos.2017.02.010

# The relationship between platelet size and the B′ infrared peak of natural diamonds revisited

L. Speich[a,*], S.C. Kohn[a], R. Wirth[b], G.P. Bulanova[a], C.B. Smith[a]

[a] *School of Earth Sciences, University of Bristol, Wills Memorial Building, Queens Road, Bristol BS8 1RJ, United Kingdom*
[b] *Helmholtz Centre Potsdam, GFZ German Research Centre for Geosciences, Telegrafenberg, 14473 Potsdam, Germany*

**Abstract**

Platelets in diamond are extended planar defects that are thought to be generated during the nitrogen aggregation process in type Ia diamonds. They were subjected to intensive research during the 1980s and 1990s but the techniques used for observation of defects in diamond have improved since that time and new insights can be gained by further study. This study combines high resolution Fourier Transform Infrared (FTIR) analysis, with an emphasis on the main platelet peak, and transmission electron microscopic (TEM) imaging. By performing TEM and FTIR analyses on volumes of diamond that were closely spatially related it is shown that the average platelet diameter, D, follows the relationship $D = \frac{a}{x-b}$ where x is the position of the platelet peak in the infrared spectrum, a is a constant and b is the minimum position of the platelet peak. The best fit to the data is obtained if a value of b = 1360 $cm^{-1}$ is used, giving a fitted value of a = 221. The observed variation in infrared (IR) peak width can also be explained in terms of this relationship. Additionally, platelet morphology was found to vary according to diameter with large platelets being more elongated. The tendency to become more elongated can be described by the empirical equation $AR = \frac{11.9}{D+19.6} + 0.4$ where AR is the aspect ratio. Using the relationships established here, it will be possible to study platelet abundance and size as a function of parameters such as nitrogen concentration, nitrogen aggregation and diamond residence time in the mantle. This work therefore will open up new methods for constraining the geological history of diamonds of different parageneses and from different localities.

*Keywords:* diamond, platelets, FTIR, TEM

*Corresponding author
*Email addresses:* ls13943@my.bristol.ac.uk (L. Speich), simon.kohn@bristol.ac.uk (S.C. Kohn), wirth@gfz-potsdam.de (R. Wirth), g.bulanova@bristol.ac.uk (G.P. Bulanova), chris_b_smith@btopenworld.com (C.B. Smith)

## 1. Introduction

Platelets are extended planar defects found only in type Ia diamond that contains nitrogen in its aggregated forms. They are among the most common defects in natural diamond. The abundance, size and shape of platelets have the potential to be used to elucidate the geological history of natural diamonds. Currently, a lower than expected concentration of platelets is often cited as evidence for short-lived high temperature events (e.g. Melton et al., 2013; Hunt et al., 2009). This interpretation is based on experimental results by Evans et al. (1995). However, much more detailed information could be extracted if the controls on platelet evolution were better understood. A first step towards this goal is to quantify the relation between the position, width and symmetry of the main platelet related infrared (IR) feature, the so-called B′ absorption, and platelet morphology. In addition, an attempt was made to derive platelet densities and the concentration of self-interstitials within platelets from the integrated area of the B′ absorption.

Platelets were discovered in the 1940s because they lead to anomalous 'spikes' in X-ray diffraction measurements that could not be reconciled with the structure of pure diamond (Raman and Nilakantan, 1940). Later, the ca. 1370 $cm^{-1}$ infrared absorption peak was also attributed to platelets and its intensity was shown to be proportional to the anomalous X-ray spikes (Sobolev et al., 1969). The underlying structure and chemical composition, however, are still subject to some debate (e.g. Goss et al., 2003; Humble, 1982; Lang, 1964; Woods, 1986). Platelet formation is associated with the production of B-centres as part of the sequence of nitrogen aggregation. As a consequence, the integrated intensity of the B′ peak is proportional to the absorption due to B centres in the majority of diamonds (Woods, 1986). In some diamonds, however, the platelet peak is less intense than expected for a given concentration of B centres. This is considered to be the result of the breakdown of platelets at high temperatures or under plastic deformation (Woods, 1986).

Because of this connection between the formation of B centres and platelets it was long thought that the latter are composed of nitrogen atoms (e.g. Lang, 1964). However, it is widely accepted today that they are thin layers of carbon self-interstitials inserted into {100} lattice planes (Humble, 1982; Goss et al., 2003) and in some cases contain variable amounts of nitrogen as an impurity (e.g. Fallon et al., 1995). This agrees with mass balance considerations: The formation of a B centre ($VN_4$) from two A centres ($N_2$) requires vacancies, making the additional carbon atom available for platelet growth. No nitrogen is released in the process.

The size of these defects can range from below 10 nm to a few microns (Kiflawi and Lang, 1977; Woods, 1976). The latter have been referred to as 'giant platelets' in the past (e.g. Woods, 1976) that can be seen in cathodoluminescence (CL) images of diamond (e.g. Collins and Woods, 1982). Platelets of up to 2 $\mu$m in size have been observed with CL in our laboratory at the University of Bristol.

The infrared platelet peak is known to vary in size and shape (Woods, 1986).

Sobolev et al. (1969) established that the position of the peak maximum is sample dependent and occurs within the range 1358-1378 $cm^{-1}$. They also demonstrated that peak position is a function of platelet diameter using FTIR and TEM data from Evans and Phaal (1962). This was confirmed and examined in more depth by Clackson et al. (1990), who determined average platelet radii by both X-ray topography and TEM imaging and combined these results with FTIR spectroscopy. Theoretical calculations by Goss et al. (2003) support this interpretation and predict a comparable downward shift in frequency of the peak for large platelets. Using similar methods to Clackson et al. (1990), Sumida and Lang (1988) found a correlation between the platelet area per unit volume of diamond, or platelet 'density', and the area of the B′ absorption. Thus, FTIR can be used as a relatively cheap and quick tool to assess properties of the platelet population in diamonds. However, the majority of studies on platelets were conducted more than two decades ago. With recent developments in analytical techniques, our understanding of the relationship between platelet characteristics and the B′ absorption can be improved by revisiting previous findings. In addition, other descriptors of the platelet peak, such as its width and symmetry, and their relation to properties of the platelets have been neglected in the past. Woods (1986) showed that the width measured at half height changes with the wavenumber of the peak maximum with broader peaks occurring at higher wavenumbers. It was hypothesised by several authors (Sobolev et al., 1969; Kiflawi et al., 1998) that the width of the B′ band could be related to platelet size distribution, as peak position is a function of average platelet size.

## 2. Materials and Methods

### *2.1. Sample preparation*

Six diamonds were selected from our collection based on previous FTIR results, with the intention of sampling a wide range of platelet shapes and sizes. The selection includes diamonds from the Mir mine (Siberia), Bunder (India), Argyle (Australia), Murowa (Zimbabwe), and Diavik (Canada) (see table 1). More information on these samples and their origin and provenance can be found elsewhere (Mir 679 and 1164: Bulanova, 1995; Bunder 09: Smith et al., submitted; Arg 78: Bulanova et al., in review; for general information on diamonds from Murowa and Diavik see Smith et al., 2009; Bulanova et al., submitted; Donnelly et al., 2007, respectively). All samples were polished on two sides parallel to {110} yielding thin, central plates with thicknesses between approximately 350 and 800 $\mu$m but most plates being less than 600 $\mu$m thick. Using sufficiently thin plates of the right orientation is crucial for high resolution FTIR analysis of diamond as outlined by Kohn et al. (2016). In diamonds with octahedral zonation, growth zones are perpendicular to {110} (Bulanova et al., 2005). Additionally, unlike FTIR, which uses transmitted light and hence samples the full thickness of the plate, the foils produced for TEM analysis only span a few microns in depth. Sample orientation and thickness are therefore essential factors in ensuring that the same sample volume is analysed with both techniques.

### 2.2. TEM

From each of the six selected diamonds, between one and three thin foils were prepared for TEM analysis at the German Research Centre for Geoscience (GFZ), Potsdam using a FEI FIB 200 TEM Focused Ion Beam (FIB) device. Details of the FIB sample preparation are given in Wirth (2009). The foils are, on average, approximately 150 nm thick. Subsequently, scanning transmission (STEM) images (high-angle annular dark-field HAADF imaging Z-contrast plus diffraction contrast) were obtained with a FEI Tecnai G2 F20 X-Twin TEM. First, an overview image of each foil was taken at low magnification, followed by higher magnification images of different parts of the foil.

As has been outlined by Woods (1986) and Clackson et al. (1990), the best sample orientation for studying platelets is parallel to {110}. Because platelets lie on {100} planes, in a thin foil of {110}-orientation, two sets of platelets form a 45° angle with the foil, the third one is perpendicular to it and will be visible as thin, straight lines in the TEM image. Hence, assuming that the platelets are equally distributed between the three {100} lattice planes, two thirds of the platelet population can be observed in full if the viewing plane is {110}. Consequently, the samples were tilted to this orientation where possible, which was confirmed with diffraction images.

### 2.3. FTIR

All diamonds were mounted on a knife-edge aperture for Fourier Transform Infrared (FTIR) spectroscopy with a Thermo iN10 MX infrared microscope at the University of Bristol. Spectra were obtained on two to three spots near each FIB pit and averages of the results were calculated. The choice of points was guided by knowledge of the zonation of the diamond from previous high resolution FTIR maps to ensure the same zone was sampled by both FTIR and TEM. The spot size was 40 $\mu$m by 40 $\mu$m and 128 scans were performed on each spot at a spectral resolution of 2 cm$^{-1}$. All spectra were then fitted to a normalised type IIa diamond spectrum using Python (version 2.7.6), which was subsequently subtracted from the measured spectrum to provide normalisation to 1 cm diamond thickness. At the same time, a sloping linear (first order polynomial) baseline was subtracted. The area of interest (1327 to 1420 cm$^{-1}$) was then interpolated to a resolution of 0.1 cm$^{-1}$ using a cubic spline interpolation method available as part of the SciPy library (Jones et al., 2001-present). To account for strong overlap between the B′ absorption with the neighbouring 1405 cm$^{-1}$ and 1332 cm$^{-1}$ lines, three pseudovoigt functions (P(x)) of the form

$$P(x) = \eta \cdot L(x) + (1 - \eta) \cdot G(x)$$

were fitted to the spectrum simultaneously, consisting of a Lorentzian (L(x)) and a Gaussian (G(x)) contribution with $0 \leq \eta \leq 1$ (see figure 1). The position, width and height of each peak were varied using a least-squares minimisation routine (Kraft, 1988). Whereas the position of the platelet peak is variable, that of the other two neighbouring peaks can be fixed within close proximity ($\pm$ 0.5 cm$^{-1}$) of their known positions. Furthermore, the 1405 cm$^{-1}$ absorption

is due to the same defect as the stronger 3107 $cm^{-1}$ line (Woods and Collins, 1983) and the intensity of the two was found to be proportional by a factor of approximately 0.26. Hence, the peak height at 1405 $cm^{-1}$ can be constrained by fitting the 3107 $cm^{-1}$ absorption with an additional, independent pseudovoigt function and predicting the height of the 1405 $cm^{-1}$ peak from that of the 3107 $cm^{-1}$ peak, allowing for a small error. A small constant is added to the sum of the pseudovoigt functions to account for a non-zero baseline. This constant is bracketed between the lowest absorption value in the 1327-1420 $cm^{-1}$ region and zero.

In favourable cases with narrow and intense B′ absorption, the position of the platelet peak can be determined within ± 0.2 $cm^{-1}$ with this procedure. For broader and weaker peaks, accuracy can be somewhat lower. The asymmetry of the platelet peak was accounted for by fitting two half-functions of different widths but identical peak maxima and heights to the measured spectrum. To assess peak symmetry, the platelet peak is treated as a statistical distribution of intensities. The distance between the mode (i.e. the position of the peak maximum) and the mean of this distribution is used as a measure of symmetry. Negative values reflect peaks skewed towards high wavenumbers which is usually found in the platelet peak.

The platelet peak area (I(B′)) can then be calculated using the analytical solution of integrating the pseudovoigt function (P(x)):

$$I(B') = \int_{-\infty}^{\infty} P(x)dx = h_{B'} \cdot (HWHM_l + HWHM_r) \cdot (\eta \cdot \frac{\pi}{2} + (1-\eta) \cdot \sqrt{\frac{\pi}{2}})) \quad (1)$$

With the absorption value at the peak maximum $h_B$ and the half width at half maximum of the two halves of the peak $HWHM_l$ and $HWHM_r$.

### *2.4. Particle Size and Density Analysis*

In order to evaluate the size and shape of the platelets in each sample, 27 high magnification STEM images were processed with ImageJ (version 1.50g, Schneider et al., 2012). The size of edge-on platelets was measured using the 'line tool' on the original images. The orientation of the other two sets of platelets on planes at a 45° angle with respect to the {100} TEM viewing plane necessitates a geometric correction. Hence, each image was rotated and stretched by a factor of $\sqrt{2}$ parallel to the {100} plane indicated by the edge-on platelets. No interpolation of the images was permitted in these steps to preserve the scale of the images and allow the true size to be measured. Stretching the images rather than applying a mathematical correction to diameters measured on the original images has the advantage that the shape of the platelets can be observed directly. In two cases, the desired sample orientation was not achievable due to the limited range of tilt of the TEM instrument used. Measurements from these foils were left uncorrected. One of these, however (Mir 679 r), was tilted to an orientation close to {100}, i.e. the platelet plane. As a consequence, one of the three sets of platelets is subparallel to the viewing plane, whereas the other two

appear as thin lines. Thus, the size and shape of the platelets is not distorted and no correction was necessary in this case.

Because of strong variations in background contrast and platelets frequently overlapping in the images, automated particle size analysis was found to be unsuitable. Furthermore, it is crucial to exclude platelets visibly truncated by the surface of the foil so as not to bias measurements towards smaller diameters. Thus, ellipses were fitted to each platelet by hand using the 'elliptical selections tool'. ImageJ records various parameters of each ellipse, such as orientation, major and minor diameters and length and orientation of each line. From these, the platelet area (A) was calculated assuming an elliptical shape

$$A = \pi \cdot a \cdot b$$

using the major and minor radii, a and b, respectively. As a measure of average platelet size that is independent of platelet shape, the diameter of a circle of equivalent area was calculated. An average of these diameters and the length of the edge-on platelets weighted by the number measured of each type was calculated since the two generally agreed within uncertainty. Averages and standard deviations were obtained combining data from all high magnification images of each foil.

On average, about 180 platelets were measured per sample. A problem arises when platelets are very large. In such samples, only a very limited number of platelets was available which influences the reliability of these measurements. Where this was the case, all platelets within the foil were documented and measured. In most cases, however, the number of platelets far exceeds 100.

Determining the uncertainty involved in measuring the size of an object with TEM is not straightforward. However, repeat measurements of the same platelet in ImageJ typically reproduce the same value within $\pm$ 2 nm. Since all measurements were carried out by hand, there is a small spread in the orientations of the ellipses, typically less than 8° (1 $\sigma$). Furthermore, the angle between the two elliptical sets of platelets was found to be within 10° of the expected 90° after image correction. The spread in angle likely results from samples imaged at a small angle with respect to the desired {110} orientation. Both these factors produce a small additional uncertainty in diameter.

To evaluate platelet densities, platelets were counted in all high resolution images using the 'Cell Counter' plugin for ImageJ. Unlike for size measurement, all platelets were taken into account here, including truncated platelets. As an estimate of overall platelet area per sample, the number of platelets was multiplied by the average area assuming a circular shape and using the average radius. The total platelet area was then divided by the volume of diamond observed in each sample using the average foil thickness of 150 nm and multiplying by the total area observed in all images.

In some cases, where platelets are large and their overall number is small, all platelets within the foil were imaged. In other words, areas of the foil that display platelets were specifically targeted for imaging. To avoid sampling bias and give a better representation of platelet density, instead of image area, the total

| | | FTIR | | | TEM (D) | | | | | | | | | |
|---|---|---|---|---|---|---|---|---|---|---|---|---|---|---|
| | | | | | linear | | | elliptical | | | | | overall | |
| sample | | x ($cm^{-1}$) | FWHM ($cm^{-1}$) | symmetry ($cm^{-1}$) | $\mu_D$ (nm) | $\sigma_D$ (nm) | n | $\mu_D$ (nm) | $\sigma_D$ (nm) | $\mu_{AR}$ | n | $\gamma_D$ | $\mu_D$ (nm) | n |
| Mir 679 | c | 1361.6 | 10.7 | -8.2 | 154 | 93 | 6 | 109 | | 0.42 | 1 | | 147 | 7 |
| | i | 1369.1 | 13.6 | -7.7 | | | | 28* | 5 | 0.54 | 39 | | 28* | 39 |
| | r** | 1367.1 | 11.6 | -7.4 | 27 | 7 | 27 | 20 | 6 | 0.46 | 178 | | 21 | 205 |
| Arg 78 | c | 1367.2 | 13.4 | -7.3 | 30 | 10 | 156 | 31 | 7 | 0.66 | 254 | 0.05 | 31 | 410 |
| Bunder 09 | c | 1365.9 | 11.7 | -6.0 | 41 | 16 | 59 | 43 | 10 | 0.62 | 135 | 1.38 | 42 | 194 |
| | i | 1364.9 | 9.4 | -3.7 | | | | 38* | 7 | 0.50 | 101 | | 38* | 101 |
| | r | 1362.0 | 7.6 | -1.2 | 65 | 14 | 2 | 146 | | 0.46 | 1 | | 92 | 3 |
| DVK 160 | i | 1363.6 | 10.9 | -5.2 | 119 | 52 | 7 | 79*** | 29 | 0.33 | 16 | | 79*** | 23 |
| Mir 1164 | r | 1369.5 | 14.2 | -10.0 | 17 | 5 | 101 | 25 | 7 | 0.71 | 472 | 0.19 | 24 | 573 |
| Mur 235 | c | 1364.3 | 9.8 | -4.4 | 42 | 16 | 195 | 43 | 9 | 0.63 | 235 | -0.31 | 43 | 430 |
| | i | 1363.2 | 8.0 | -2.6 | 67 | 28 | 74 | 68 | 14 | 0.57 | 55 | | 68 | 129 |
| | r | 1361.5 | 6.8 | -0.7 | 228 | 103 | 9 | 85 | 43 | 0.52 | 11 | | 149 | 20 |

Table 1: Position and shape of B′ IR peak and size and shape data of platelets from TEM. c = core, i = intermediate, r = rim. x = platelet peak position, FWHM = full width at half maximum, symmetry = distance between platelet peak position and mean wavenumber, $\mu_D$ = average diameter, $\sigma_D$: standard deviation of the size distribution, $\mu_{AR}$ = average aspect ratio ($D_{minor}/D_{major}$), $\gamma_D$ = skewness of the size distribution for linear and elliptical platelets. Overall values are weighted averages of both types of platelets. * uncorrected due to unsuitable sample orientation, ** sample oriented parallel to {100}, *** uncorrected results from bright field images.

area of the foil was used. Hence, the platelet area per unit volume of diamond or platelet 'density' was obtained.

It should be noted that this approach is a simplification and does not account for the non-linear relationship between platelet radius and area. A symmetrical distribution of sizes does not correspond to a symmetrical distribution of areas since area is proportional to $r^2$. Instead, the latter would be skewed towards higher values around a mean value that is slightly higher than the square of the mean radius. Thus, the total platelet density will be underestimated by a small amount.

## 3. Results and Discussion

FTIR and TEM data for all samples are summarised in table 1. Representative examples of typical TEM images are given in figure 2 and typical size distributions are shown in figure 3. Overall, platelet diameters were found to vary between about 15 and 200 nm, with the majority of platelets not exceeding 150 nm. Most samples appeared to be homogeneous on the scale of the FIB sections (ca. 18 $\mu$m x 7 $\mu$m). In one case, platelets occurred predominantly in the vicinity of a low-angle grain boundary, whereas in the case of Arg 78 platelets are concentrated in a band of a few hundred nanometers width. The latter sample is highly platelet degraded and contains not only platelets but abundant dislocation loops. One sample in particular (Mir 679) was found to be very inhomogeneous overall in terms of platelet population, containing platelets of both extremes of the size range in foils from core and rim areas, respectively, illustrating the importance of spatially resolved analysis of diamonds.

For platelet peaks occurring above ca. 1367 $cm^{-1}$ (i.e. small platelets), our data agrees well with previous findings (see figure 4). Below this value, our data predicts larger platelets for any given peak position than the data by Clackson et al. (1990). One possible explanation for this is the improvement in analytical techniques over the last two decades. Modern FTIR spectrometers allow measurements at very high spatial and spectral resolutions to be carried out within minutes making high resolution mapping feasible. Furthermore, the method to produce thin foils for TEM analysis here provides better control over the sample volume analysed, ensuring that close sample volumes are analysed with both techniques.

Previous studies have suggested various types of relationships between the position of the B′ peak (x, in $cm^{-1}$) and average platelet diameter (D, in nm), such as parabolic (Vasilev and Sofroneev, 2007) or linear (Clackson et al., 1990) functions, the latter using platelet peak positions recorded in wavelength rather than wavenumber. For our data, a reciprocal relationship of the form

$$D = \frac{a}{x - b} \tag{2}$$

appears to result in a reasonable fit (see figure 4). Clackson et al. (1990) propose that the vibrational frequency of a platelet is influenced by the ratio of atoms residing at the edge of the defect relative to atoms at the centre. This ratio is proportional to the reciprocal diameter of the platelet. Accepting b in equation 2 as the minimum position of the platelet peak reflecting a very large platelet, the shift of the peak relative to this value is proportional to the reciprocal of the diameter. However, using the widely reported minimum value of 1358 $cm^{-1}$ (e.g. Sobolev et al., 1969; Goss et al., 2003) and fitting the value for a (equation 2) with a least-squares routine, does not agree well with our data. Minimum platelet peak positions between 1359 and 1360 $cm^{-1}$ lead to much better agreement (see curves 2 and 3 in figure 4).

Previously, no attempt has been made to reconcile such findings with comparable data for 'giant platelets'. Figure 4 includes a measurement of mean platelet size in CL images and the corresponding platelet peak position (sample Mir 1180). This point was not used in the fitting of equation 2 but agrees well with the fit using 1360 $cm^{-1}$ as the minimum platelet peak position.

It should be noted that platelets smaller than about 200 nm can not be detected by CL with the experimental setup and conditions used here, leading to some uncertainty in mean platelet diameter. If the platelet population is not strongly dominated by the 'giant platelets' seen in CL, the true average platelet diameter could be much lower than the measured value, driving the platelet peak towards higher wavenumbers. Furthermore, platelet peaks occurring at such low wavenumbers tend to be broad and less intense. As a consequence, determining the position of the peak maximum is less accurate than in a sharp, intense peak.

It has been suggested that platelet shape varies with size with small platelets being roughly circular (Clackson et al., 1990). With increasing size, their appearance changes from circular to elliptical and then lath-shaped and increas-

ingly elongated in <110>. Our data confirms these observations with the exception that medium-sized platelets have the shape of rounded rectangles rather than ellipses (see figure 2). A simple way of quantifying and comparing the shape of particles is aspect ratio (AR). Here, the average ratio of minor over major diameter of the platelets was used (see figure 5a). There is a general tendency for larger platelets to be more elongated. Assuming that the smallest platelets are perfectly circular with an aspect ratio of 1, the following empirical relationship was obtained by least-squares fitting:

$$AR = \frac{11.9}{D + 19.6} + 0.4 \tag{3}$$

where D is the mean platelet diameter in nm. Equation 3 implies that an infinitely large platelet would have an aspect ratio of 0.4. Size has little influence on aspect ratio for platelets larger than ca. 150 nm. Unpublished CL images by J. Milledge (pers. comm.) show 'giant platelets' with an average aspect ratio of 0.87, demonstrating that these are no more elongated than the largest platelets observed in TEM. However, it should be noted that the orientation of the sample was not recorded. Thus, it is not possible to comment further on the apparent discrepancy between the aspect ratio predicted for large platelets by equation 3 and the observed value.

The full width at half height of the platelet peak is known to increase with increasing wavenumber of the peak maximum (Woods, 1986), or with decreasing platelet size. It has been suggested that broad platelet peaks could indicate a wider size distribution (Sobolev et al., 1969; Kiflawi et al., 1998). Examples of typical size distributions are shown in figure 3. The relative standard deviation of platelet sizes for each sample can be used to describe the width of the distribution. As can be seen from figure 5b however, the relative standard deviation is roughly constant over the range of sizes observed. This suggests that the width of the platelet peak is not controlled by platelet size distribution.
In fact, the variation in width could be simply a consequence of the curvature of the function in equation 2 changing with platelet diameter, evident also in figure 4. For small platelets, a given distribution in sizes results in a larger spread of frequencies than a distribution of the same width of small platelets.

Equation 2 and the favoured coefficients of a = 221 and b = 1360 can be employed to predict the mean platelet size from the measured platelet peak positions in table 1. Adding and subtracting a relative standard deviation of 30% from this size, 'minimum' and 'maximum' platelet peak positions can be determined using the same equation. The difference between these two values, the predicted full width at half maximum, is lower than the measured peak width. Adding a constant value of 6.1 $cm^{-1}$ results in a good correlation (see figure 5c). Hence, the width of the B′ absorption is determined by the relationship between platelet size and peak position and an additional constant source of broadening.

The symmetry of the B′ absorption is known to vary, with peaks at high wavenumbers generally being more asymmetric (Woods, 1986). However, this is unlikely a result of the skewness of platelet size distribution as there appears to be no correlation between the two in our dataset. In fact, where the number

of platelets measured is high enough to make such statements, size distributions are only marginally and non-systematically skewed to either smaller or larger platelets (see figure 3 and table 1). Furthermore, the most asymmetric platelet peak was found for sample Mir 1164, whereas the platelet size distribution in this sample is very symmetric around the mean. Hence, our data suggests that it is unlikely that the asymmetry of the platelet peak is caused by an uneven distribution of defect sizes.

The approach suggested above to predict the width of the platelet peak can theoretically be applied to explain its asymmetry as well. Based on the form of equation 2 (figure 4), a symmetrical distribution of sizes would result in a wider range of frequencies at the high wavenumber side of the peak than at the low wavenumber side, i.e. the peak would be skewed towards high wavenumbers. This is the sense of skewness seen in FTIR spectra of diamonds containing platelets. So an asymmetric distribution in platelet sizes is not required to explain the observed skewness of the IR peak.

Finally, our data set can be used to re-investigate the relationship between the integrated area of the B′ absorption and platelet density first studied by Sumida and Lang (1988). FTIR peak intensities and TEM platelet abundance data are summarised in table 2. Figure 6 shows a least-squares fit to all data where the average platelet diameter was obtained from corrected images which yields

$$\rho_p = 2.41 \cdot 10^{-6} \cdot I(B') \tag{4}$$

where $\rho_p$ is the platelet density in $nm^2/nm^3$ and I(B′) is the platelet peak area in $cm^{-2}$. The scatter in figure 6a can be explained in terms of variation in thickness of the foils. As expected, all points derived from uncorrected mean diameters fall below the dashed line. The uncorrected point closest to the line represents the rim sample of Mir-679, the orientation of which was near {100}. Our equation 4 is similar to equation 4 in Sumida and Lang (1988) who obtained a correlation factor of $9.0 \pm 2.1 \cdot 10^{-6} cm^2/nm$ for the same relationship. However, Sumida and Lang (1988) used a different method to calculate platelet peak area and their result is based on a single sample which could, at least partially, account for the apparent discrepancy between their data and this study.

From platelet density, the concentration of interstitials in platelets can be calculated. The distance between two neighbouring atoms within the platelet plane of 0.2517 nm was measured in CrystalMaker (version 9.2.7) in accordance with platelet models proposed by Goss et al. (2003) that are based on the Humble platelet structure (Humble, 1982). It follows, that the density of atoms in the platelet plane is 7.859 $nm^{-2}$. Thus, the number of interstitials per unit volume of diamond is this value multiplied by platelet density, $\rho_p$ in $nm^2/nm^3$, assuming that platelets consist of a monolayer of interstitials.

Diamond contains 8 carbon atoms on lattice sites per unit cell. Using the unit cell parameter of diamond, 0.3560 nm, this yields $0.17731 \cdot 10^3$ $nm^{-3}$. Hence, the following two equations can be used to calculate the concentration of interstitials in platelets ($[c_i]$ in at. prop.) from the platelet area per unit volume of diamond

($\rho_p$ in $nm^2/nm^3$) and the integrated area of the IR platelet absorption (I(B′) in $cm^{-2}$). $\rho_p$ in equation 5 has been substituted using equation 4 to obtain equation 6.

$$[C_i] = 89.03 \cdot 10^{-3} \cdot \rho_p \tag{5}$$

$$[C_i] = 214.56 \cdot 10^{-9} \cdot I(B') \tag{6}$$

Assuming that (i) all interstitials associated with nitrogen aggregation are incorporated into platelets, that (ii) the number of interstitials derived from other processes is negligible and that (iii) platelets contain no species other than carbon, $[C_i]$ should be a quarter of the concentration of nitrogen in B centres ($[N_B]$) in regular diamonds. As can be seen in table 2 and figure 6b, the $[C_i]/[N_B]$ ratio is close to 0.25 for only some of the other samples. The overall average is only 0.13 (excluding Arg-78 which is irregular), thus underestimating interstitial concentration in platelets by a factor of 2. However, the lowest values of $[C_i]/[N_B]$ correspond to samples where the total number of platelets measured and counted is low, increasing the uncertainty in platelet size and density and hence interstitial concentration. Excluding all samples where the platelet count is below 100 yields an average $[C_i]/[N_B]$ ratio of 0.16, still lower than expected.

It is not clear whether this discrepancy is significant. It might be that some of the assumptions in the calculations are incorrect (for example, the assumed thickness of the FIB sections). Alternatively, there may be another sink for interstitial carbon atoms in addition to platelets, or potentially the Humble model for the structure of platelets underestimates underestimates the interstitial concentration per unit area.

## 4. Conclusions

The main success of this paper is the improved correlation between the position of the IR platelet peak and the mean diameter of these defects. Using equation 2, FTIR results can now be used with confidence as a proxy for platelet size. Furthermore, it can be shown that the shape of platelets varies as size increases; Large platelets are more elongated and angular than small platelets. However, in light of our results, it is unlikely that the variations in width and degree of symmetry of the IR platelet peak are caused by differences in the shape of the platelet size distribution. Instead, the variation in width is a direct consequence of the reciprocal nature of the relationship between platelet size and peak position. This considerably simplifies the interpretation of infrared spectroscopic data of platelet bearing diamonds.

Finally, the relationship between platelet area per unit volume of diamond and the integrated area of the B′ absorption was revisited. The area of observed platelets is lower by a factor of about 2 than expected on the basis of the concentration of nitrogen in B-centres, using the Humble (1982) structure for the platelet defect. However, a number of assumptions are required for the

| | | FTIR | | TEM | | | | | |
|---|---|---|---|---|---|---|---|---|---|
| sample | | I(B′) $cm^{-2}$ | $[N_B]$ (ppm) | $\mu_D$ (nm) | $A_{img}$ $(10^3 nm^2)$ | n | $\rho_p$ $(10^{-3} nm^2/nm^3)$ | $[C_i]$ ppm | $[C_i]/[N_B]$ |
| Mir 679 | c | 74 | 159 | 147 | 19307 | 12 | 0.07032 | 6 | 0.04 |
| | i | 75 | 106 | 28* | 4400 | 212 | 0.19778 | 18 | 0.17 |
| | r** | 114 | 192 | 21 | 2202 | 206 | 0.21599 | 19 | 0.10 |
| Arg 78 | c | 127 | 1100 | 31 | 6716 | 626 | 0.46901 | 42 | 0.04 |
| Bunder 09 | c | 479 | 603 | 42 | 4682 | 425 | 0.83841 | 75 | 0.12 |
| | i | 394 | 489 | 38* | 4396 | 362 | 0.62267 | 55 | 0.11 |
| | r | 42 | 51 | 92 | 14068 | 14 | 0.04410 | 4 | 0.08 |
| DVK 160 | i | 119 | 122 | 79*** | 117832 | 23 | 0.00638 | 1 | 0.01 |
| Mir 1164 | r | 104 | 163 | 24 | 8086 | 968 | 0.36106 | 32 | 0.20 |
| Mur 235 | c | 422 | 547 | 43 | 4403 | 594 | 1.30608 | 116 | 0.21 |
| | i | 298 | 384 | 68 | 6613 | 219 | 0.80183 | 71 | 0.19 |
| | r | 89 | 129 | 149 | 27439 | 42 | 0.17793 | 16 | 0.25 |

Table 2: Platelet peak area and $[N_B]$ concentration from IR and platelet density and calculated interstitial concentrations from TEM. c = core, i = intermediate, r = rim. I(B′) = integrated area of the platelet peak calculated according to equation 1, $[N_B]$ = concentration of N in B centres obtained by IR spectroscopy, $\mu_D$ = average diameter (overall values, taken from table 1), $A_{img}$ = total image area studied, n = total number of platelets counted, $\rho_p$ = platelet area per unit volume of diamond (population density), $[C_i]$ = concentration of interstitials in platelets calculated using equation 5. * uncorrected due to unsuitable sample orientation, ** sample oriented parallel to {100}, *** uncorrected results from bright field images.

calculation, so further study would be needed to confirm the discrepancy before alternative explanations are proposed.

Modern FTIR spectrometers with high-resolution mapping capabilities allow thousands of spectra to be collected on a single diamond sample within a few hours, and in each spectrum the platelet peak position can now be interpreted in terms of platelet size. This capability allows the platelet abundance and size to be studied as a function of parameters such as nitrogen concentration, nitrogen aggregation and diamond residence time in the mantle. That work is currently under way in our laboratory and will open up new methods for constraining the geological history of diamonds of different parageneses and from different localities.

## 5. Acknowledgements

We thank A. Schreiber (GFZ, German Research Centre for Geosciences, Potsdam) for her skilful preparation of the TEM samples, Rio Tinto and the Diamond and Precious Metal Institute (Yakutsk) for the provision of samples and David Fisher (De Beers UK Limited) for fruitful discussions and comments. LS thanks NERC and De Beers UK Limited for financial support.

In addition, we thank Oded Navon and two anonymous reviewers for their constructive comments that helped to improve this paper.

## References


Bulanova, G., Smith, C., Kohn, S., Pearson, D., Davy, A., Marks, A., McKay, A., submitted. Diamonds from Murowa kimberlites formation within extremely depleted and metasomatised Zimbabwean peridotitic subcontinental mantle. Economic Geology.

Bulanova, G. P., 1995. The formation of diamond. Journal of Geochemical Exploration 53 (1-3), 1–23.

Bulanova, G. P., Speich, L., Smith, C. B., Gaillou, E., Kohn, S. C., Wibberley, E., Chapman, J. G., Howell, D., Davy, A. T., in review. The unique nature of Argyle fancy diamonds: internal structure, paragenesis and reasons for color. Economic Geology.

Bulanova, G. P., Varshavsky, A. V., Kotegov, V. A., 2005. A venture into the interior of natural diamond: genetic information and implications for the gem industry: part I: the main types of internal growth structures. Journal of Gemmology 29 (7/8), 377.

Clackson, S. G., Moore, M., Walmsley, J. C., Woods, G. S., 1990. The relationship between platelet size and the frequency of the B′ infrared-absorption peak in Type-Ia diamond. Philosophical Magazine B-Physics of Condensed Matter Statistical Mechanics Electronic Optical and Magnetic Properties 62 (2), 115–128.

Collins, A., Woods, G., 1982. Cathodoluminescence from giant platelets, and of the 2.526 eV vibronic system, in type Ia diamonds. Philosophical Magazine B 45 (4), 385–397.

Donnelly, C. L., Stachel, T., Creighton, S., Muehlenbachs, K., Whiteford, S., 2007. Diamonds and their mineral inclusions from the A154 South pipe, Diavik Diamond Mine, Northwest Territories, Canada. Lithos 98 (1-4), 160–176.

Evans, T., Kiflawi, I., Luyten, W., Vantendeloo, G., Woods, G. S., 1995. Conversion of platelets into dislocation loops and voidite formation in type Iab diamonds. Proceedings of the Royal Society-Mathematical and Physical Sciences 449 (1936), 295–313.

Evans, T., Phaal, C., 1962. Imperfections in type I and type II diamonds. Proceedings of the Royal Society of London Series a-Mathematical and Physical Sciences 270 (1343), 538–546.

Fallon, P. J., Brown, L. M., Barry, J. C., Bruley, J., 1995. Nitrogen determination and characterization in natural diamond platelets. Philosophical Magazine A-Physics of Condensed Matter Structure Defects and Mechanical Properties 72 (1), 21–37.

Goss, J. P., Coomer, B. J., Jones, R., Fall, C. J., Briddon, P. R., Oberg, S., 2003. Extended defects in diamond: The interstitial platelet. Physical Review B 67 (16).

Humble, P., 1982. The structure and mechanism of formation of platelets in natural Type Ia diamond. Proceedings of the Royal Society of London Series A-Mathematical Physical and Engineering Sciences 381 (1780), 65–81.

Hunt, L., Stachel, T., Morton, R., Grutter, H., Creaser, R. A., 2009. The Carolina kimberlite, Brazil - insights into an unconventional diamond deposit. Lithos 112, 843–851.

Jones, E., Oliphant, T., Peterson, P., et al., 2001-present. SciPy: Open source scientific tools for Python. [Online; accessed 2016-08-15].
URL `http://www.scipy.org/`

Kiflawi, I., Bruley, J., Luyten, W., Van Tendeloo, G., 1998. 'natural' and 'man-made' platelets in type-Ia diamonds. Philosophical Magazine B-Physics of Condensed Matter Statistical Mechanics Electronic Optical and Magnetic Properties 78 (3), 299–314.

Kiflawi, I., Lang, A., 1977. Polarised infrared cathodoluminescence from platelet defects in natural diamonds. Nature 267, 36–37.

Kohn, S. C., Speich, L., Smith, C. B., Bulanova, G. P., 2016. FTIR thermochronometry of natural diamonds: A closer look. Lithos 265, 148 – 158, the Nature of Diamonds and Their Use in Earth's Study.

Kraft, D., 1988. A software package for sequential quadratic programming. Forschungsbericht / Deutsche Forschungs- und Versuchsanstalt fr Luft- und Raumfahrt. Wissenschaftliches Berichtswesen der DFVLR Vertrieb, Kln.

Lang, A. R., 1964. A proposed structure for nitrogen impurity platelets in diamond. Proceedings of the Physical Society of London 84 (5426), 871–876.

Melton, G. L., Stachel, T., Stern, R. A., Carlson, J., Harris, J. W., 2013. Infrared spectral and carbon isotopic characteristics of micro- and macro-diamonds from the Panda kimberlite (Central Slave Craton, Canada). Lithos 177, 110–119.

Raman, C. V., Nilakantan, P., 1940. Reflection of X-rays with change of frequency. Part II. The case of diamond. Proc. Indian Acad. Science Sect A 11, 389–397.

Schneider, C. A., Rasband, W. S., Eliceiri, K. W., 2012. NIH image to ImageJ: 25 years of image analysis. Nature Methods 9 (7), 671–675.

Smith, C., Bulanova, G., Kobussen, A., Burnham, A., Chapman, J., Davy, A., Sinha, K., submitted. Diamonds from the Bunder lamproites and the nature of the underlying mantle. Economic Geology.

Smith, C. B., Pearson, D. G., Bulanova, G. P., Beard, A. D., Carlson, R. W., Wittig, N., Sims, K., Chimuka, L., Muchemwa, E., 2009. Extremely depleted lithospheric mantle and diamonds beneath the southern Zimbabwe Craton. Lithos 112, 1120–1132.

Sobolev, E., Lenskaya, S., Lisoivan, V., 1969. Lamellar formations in the structure of natural diamonds. Journal of Structural Chemistry 9 (6), 917–920, translated from Zhurnal Strukturnoi Khimii, Vol. 9, No. 6, 1968, pp.10291033.

Sumida, N., Lang, A. R., 1988. On the measurement of population-density and size of platelets in Type-Ia diamond and its implications for platelet structure models. Proceedings of the Royal Society of London Series A-Mathematical Physical and Engineering Sciences 419 (1857), 235–257.

Vasilev, E. A., Sofroneev, S. V., 2007. Zoning of diamonds from the Mir kimberlite pipe: Results of fourier-transformed infrared spectroscopy. Geology of Ore Deposits 49 (8), 784–791, translated from Zapiski Rossiiskogo Mineralogicheskogo Obshchestva, 2007, Pt CXXXVI, No. 1, pp. 90101.

Wirth, R., 2009. Focused Ion Beam (FIB) combined with SEM and TEM: Advanced analytical tools for studies of chemical composition, microstructure and crystal structure in geomaterials on a nanometre scale. Chemical Geology 261 (3-4), 217–229.

Woods, G. S., 1976. Electron-microscopy of giant platelets on cube planes in diamond. Philosophical Magazine 34 (6), 993–1012.

Woods, G. S., 1986. Platelets and the infrared-absorption of Type-Ia diamonds. Proceedings of the Royal Society of London Series a-Mathematical Physical and Engineering Sciences 407 (1832), 219–238.

Woods, G. S., Collins, A. T., 1983. Infrared-absorption spectra of hydrogen complexes in Type-I diamonds. Journal of Physics and Chemistry of Solids 44 (5), 471–475.

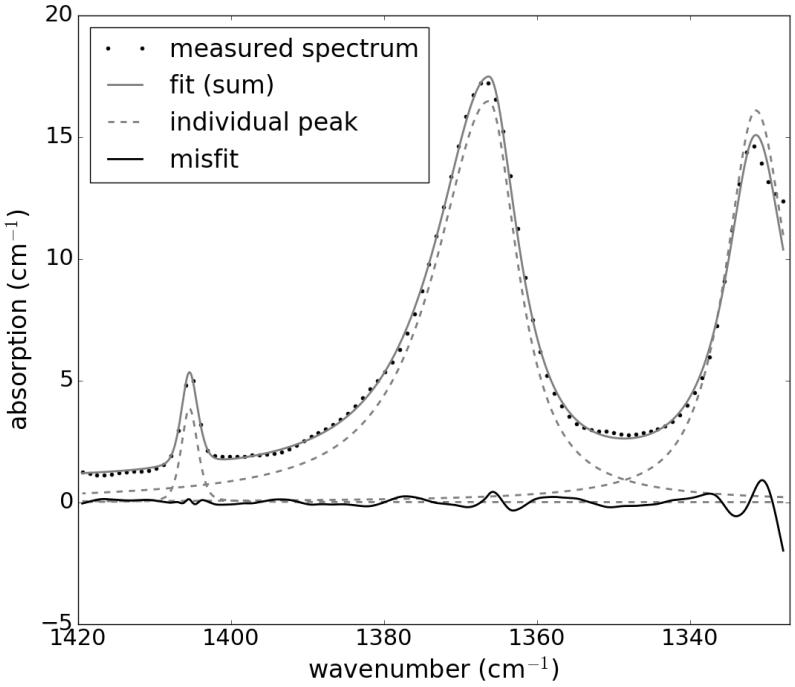


Figure 1: Example of combined pseudovoigt fit to the platelet peak region of a typical type IaAB diamond spectrum. The overlap between the 1405cm$^{-1}$ $VN_3H$ peak, the ca. 1375 cm$^{-1}$ platelet peak and the 1332 cm$^{-1}$ edge of the B spectrum is evident. To account for the asymmetry, two half-functions with identical peak position and height but different widths are fitted to the two sides of the platelet peak.

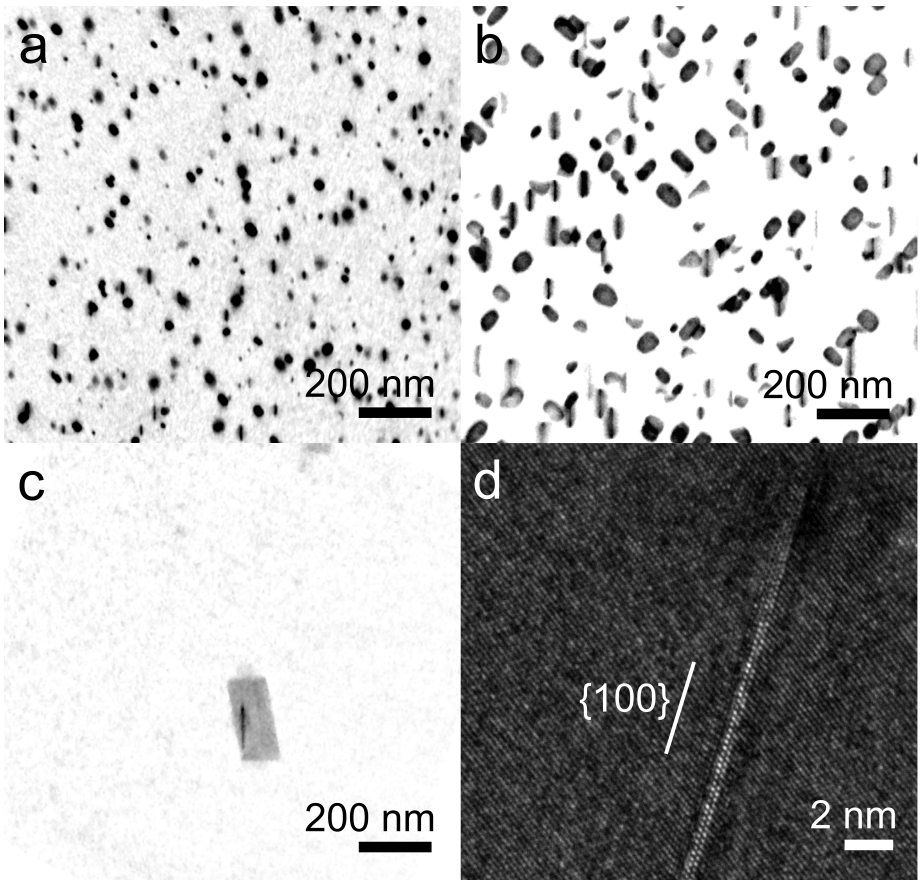


Figure 2: a)-c) Comparison of shapes in platelets of increasing size. All images are rotated and stretched by a factor of $\sqrt{2}$ parallel to {100} (see text) and inverted for clarity. a) predominantly circular platelets in Mir 1164 (average diameter: 25 nm), b) rounded rectangles (core of Murowa 235, average diameter: 43 nm), c) lath-shaped platelets (rim of Bunder 9, average diameter: 146 nm) d) HRTEM image of a very thin edge-on platelet in sample Mur 235c, the white line indicates the orientation of a {100} plane as confirmed by diffraction images.

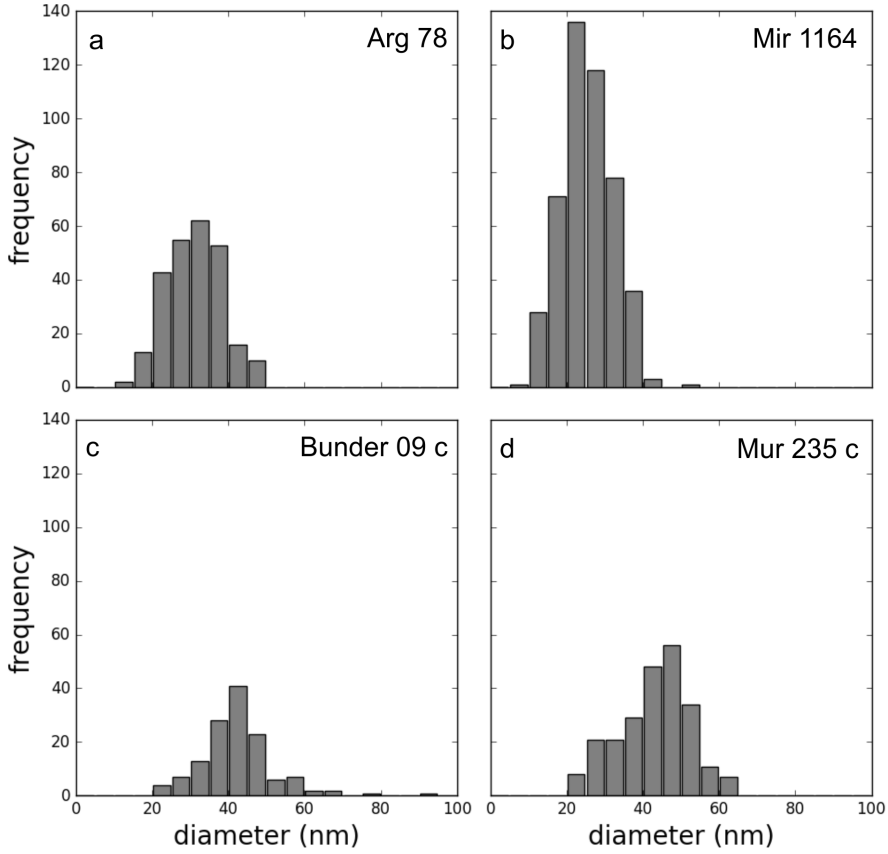


Figure 3: Typical size distributions of elliptical platelets (diameter of circle of equivalent area, see text for further explanation) for samples with sufficiently large population. a) Argyle 78, b) Mir 1164, c) Bunder 09 (core), d) Murowa 235 (core). Average diameters, platelet count and skewness of size distributions can be found in table 1.

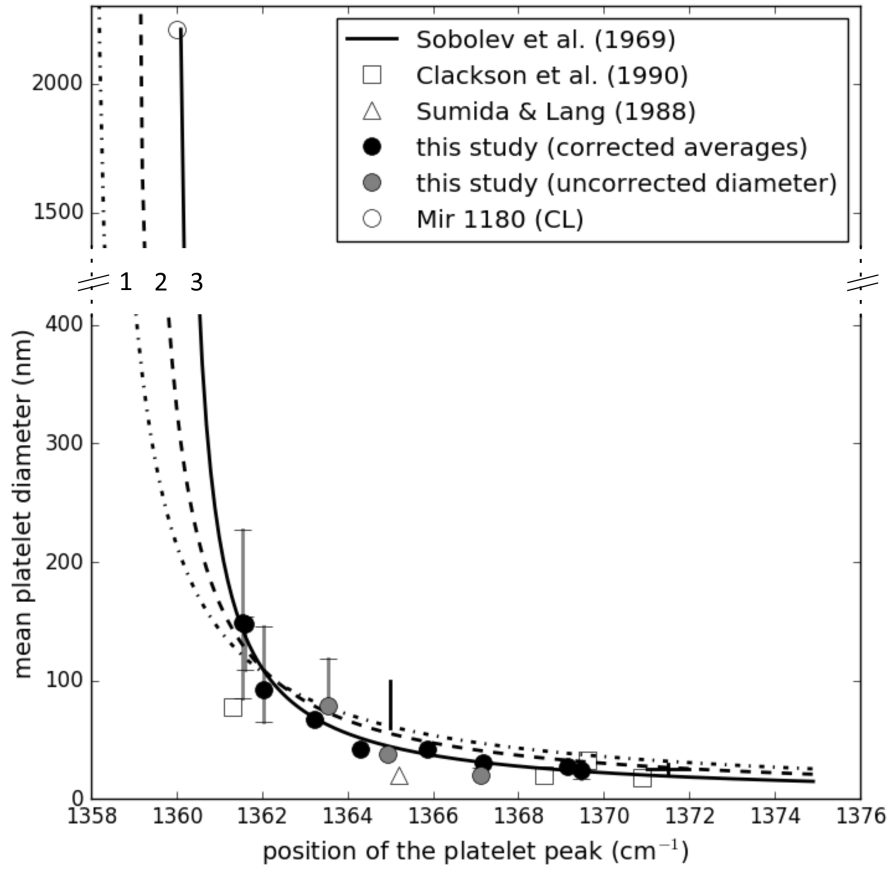


Figure 4: Variation of platelet peak position with mean platelet diameter. Dashed lines: least-squares fits to corrected averages based on equation 1 using different values for b to obtain a: 1) a = 429, b = 1358; 2) a = 331, b = 1359; 3) a = 221, b = 1360. Mir 1180 (CL) was not included in the fit but agrees well with 3). Grey vertical lines indicate platelet sizes measured using elliptical and linear subset for the same sample. Note break in scale.

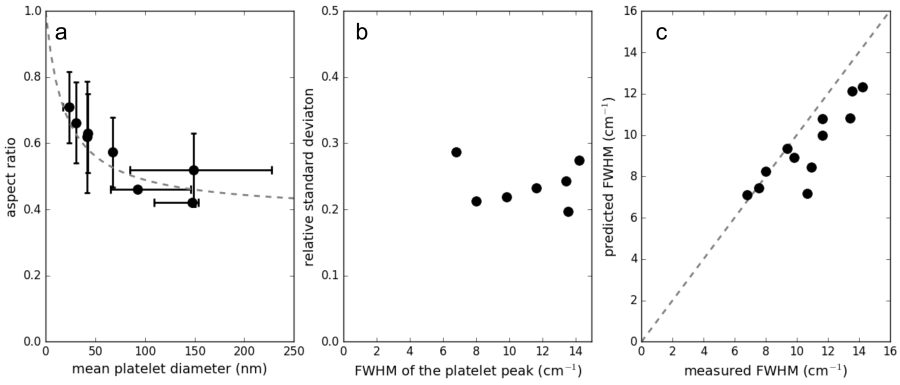


Figure 5: a) Relationship between aspect ratio (ratio of minor over major diameter) and mean platelet diameter (dashed curve: least-squares fit to data yielding equation 3, vertical error bars represent 1 $\sigma_{AR}$, horizontal lines indicate measurements for the linear and elliptical subsets of platelets in each sample). b) Relationship between relative standard deviation (normalised to average platelet diameter) and width of the platelet peak. c) Modelling platelet peak width using equation 2 to predict mean platelet size from peak positions in table 1 and 'minimum' and 'maximum' peak positions for $D_{pred} \pm 30\%$. Error bars for FWHM in b) and c) are approximately equal to symbol size.

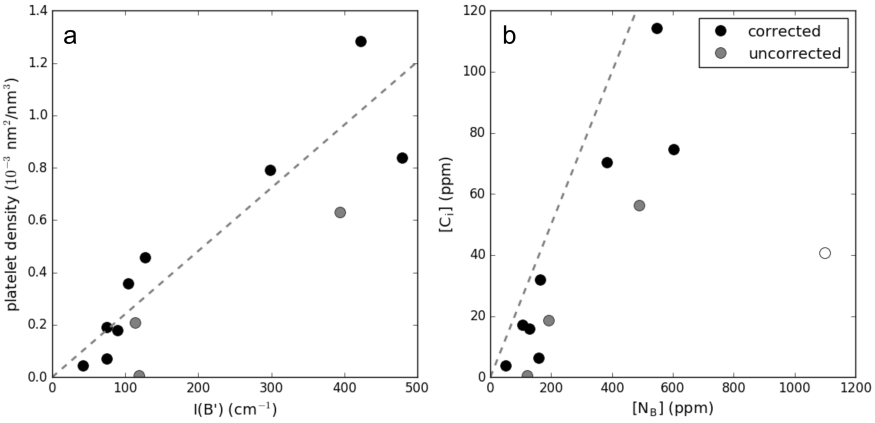


Figure 6: a

) Variation of platelet density (total platelet area per unit volume of diamond, assuming an average thickness of the observed sample volume of 150 nm) with the integrated area of the platelet peak obtained using equation 1. Dashed line: best fit to the corrected data ($R^2$: 0.84). b) Relationship between concentration of interstitials in platelets calculated according to equation 5 and concentration of N in B-centres. Dashed line: expected $[C_i]/[N_B]$ of 1/4, white symbol: sample Arg 78 (irregular).